1   # A unified physiological framework of transitions between seizures,

2   ## sustained ictal activity and depolarization block at the single neuron level

3   Short Title: Dynamics of pathologic behaviors at single neuron level

4   Damien Depannemaecker[1,2,#a,*], Anton Ivanov[1], Davide Lillo[1], Len Spek[1,#b], Christophe

5   Bernard[1, ¶], and Viktor Jirsa[1,¶]

6   [1]Aix Marseille Univ, INSERM, INS, Institut des Neurosciences des Systèmes, Marseille,

7   France

8   [2]Disciplina de Neurociência, Departamento de Neurologia e Neurocirurgia, Universidade de

9   Federal de São Paulo, São Paulo, Brazil.

10   [#a]actual addresses: Department of Integrative and Computational Neuroscience, Institut

11   Neuro-PSI, CNRS, Gif-sur-Yvette, France

12   [#b]actual addresses: Department of Applied Mathematics, University of Twente, Enschede, The

13   Netherlands

14   *Corresponding author: damien.d@cnrs.fr

15   ¶equally contributing last authors

16

17

18

19

20

21

22

1

Abstract

The majority of seizures recorded in humans and experimental animal models can be described by a generic phenomenological mathematical model, The Epileptor. In this model, seizure-like events (SLEs) are driven by a slow variable and occur via saddle node (SN) and homoclinic bifurcations at seizure onset and offset, respectively. Here we investigated SLEs at the single cell level using a biophysically relevant neuron model including a slow/fast system of four equations. The two equations for the slow subsystem describe ion concentration variations and the two equations of the fast subsystem delineate the electrophysiological activities of the neuron. Using extracellular K^+ as a slow variable, we report that SLEs with SN/homoclinic bifurcations can readily occur at the single cell level when extracellular K^+ reaches a critical value. In patients and experimental models, seizures can also evolve into sustained ictal activity (SIA) and, depolarization block (DB), activities which are also parts of the dynamic repertoire of the Epileptor. Increasing extracellular concentration of K^+ in the model to values found during experimental status epilepticus and DB, we show that SIA and DB can also occur at the single cell level. Thus, seizures, SIA and DB, which have been first identified as network events, can exist in a unified framework of a biophysical model at the single neuron level and exhibit similar dynamics as observed in the Epileptor.

Author Summary

Epilepsy is a neurological disorder characterized by the occurrence of seizures. Seizures have been characterized in patients in experimental models at both macroscopic and microscopic scales using electrophysiological recordings. Experimental works allowed the establishment of a detailed taxonomy of seizures, which can be described by mathematical models. We can distinguish two main types of models. Phenomenological (generic) models have few parameters and variables and permit detailed dynamical studies often capturing a majority of activities observed in experimental conditions. But they also have abstract parameters, making biological interpretation difficult. Biophysical models, on the other hand, use a large number of variables and parameters due to the complexity of the biological systems they represent. Because of the multiplicity of solutions, it is difficult to extract general dynamical rules. In the present work, we integrate both approaches and reduce a detailed biophysical model to sufficiently low-dimensional equations, and thus maintaining the advantages of a generic model. We propose, at the single cell level, a unified framework of different pathological activities that are seizures, depolarization block, and sustained ictal activity.

Introduction

Seizures are part of the repertoire of built-in activities of neuronal networks as they can be triggered in most brain regions from most species (Jirsa et al. 2014). Several conceptual frameworks have been proposed to explain seizure dynamics (Naze 2015; Naze et al. 2015; Soltesz and Staley 2008; Staley 2015; Stefanescu et al. 2012; Y. Wang et al. 2017; Wendling et al. 2016). The predominant framework assumes that the majority of seizure onsets and offsets correspond to bifurcations in the electrophysical variables (Jirsa et al. 2014; Saggio et al. 2017), although there exist other non-bifurcation types (Blenkinsop et al. 2012). This framework has been generalized by Saggio and colleagues (Saggio et al. 2017, 2020). A phenomenological mathematical model, called The Epileptor, describes the dynamics of a majority of seizures recorded in drug-resistant patients, and most seizures recorded in experimental models (Jirsa et al. 2014; Saggio et al. 2020). A qualitative analysis of the Epileptor reveals that seizures, SIA and DB co-exist, and that multiple types of transitions from one type of activity to the other are possible, as verified experimentally (El Houssaini et al. 2015; Houssaini et al. 2020; Saggio et al. 2017). Since it is phenomenological, the Epileptor model does not provide direct insight regarding underlying biophysical mechanisms. The phenomenological model imposes strong constrains in terms of dynamics. Numerous neuronal network models, including biophysically realistic ones, have been developed to study seizures, SIA or DB mechanisms (Holt and Netoff 2013; V.K. Jirsa et al. 2017; Kim and Nykamp 2017; Krishnan et al. 2015; Lytton 2008; Naze 2015; Proix et al. 2014; Stefanescu et al. 2012; Traub and Wong 1982). These models contain too many parameters and variables to perform a detailed bifurcation analysis, thus preventing bridging the gap between phenomenological and biophysical approaches. However, with the guidance of phenomenological modeling, design of neuronal spiking network including several biophysical features has been performed (Naze et al. 2015). In this work, transitions between states of the neuronal network are ensured by slow variable representing extracellular environmental fluctuation.

83   Although seizures and DB are generally observed at the neuronal network scale, their

84   dynamical equivalence can be found at the single cell level (Bikson et al. 2003; Bragin et al.

85   1997; Chizhov et al. 2018; Cressman et al. 2009; Hübel and Dahlem 2014; Kager et al. 2000;

86   Lietsche et al. 2016; McCormick and Contreras 2001), which can be used to study human

87   epilepsy (Merricks et al. 2015; Tankus 2016; Truccolo et al. 2011). Moreover, previous works

88   (Viktor K. Jirsa and Stefanescu 2011; Montbrió et al. 2015; Naze et al. 2015) show that

89   dynamical features are preserved when going from the weakly coupled network to the single

90   cell level. It therefore seems appropriate to consider a biophysical model at the single cell scale

91   exhibiting dynamic properties identified in the generic model and in which the transitions

92   between the different states are provided by a slow variable describing the variations within

93   the extracellular milieu. Bursting activity in neurons can be described in terms of bifurcations

94   (E. Izhikevich 2007; E. M. Izhikevich 2000), and different single cell biophysical models have

95   been proposed, which can model SLE and DB, but not SIA (Barreto and Cressman 2011;

96   Chizhov et al. 2018; Cressman et al. 2009; Hübel and Dahlem 2014; Kager et al. 2000;

97   Øyehaug et al. 2012; Ullah and Schiff 2010; Y Wei et al. 2014; Yina Wei, Ullah, Ingram, et al.

98   2014), although, to the best of our knowledge, these activities have not been observed

99   experimentally in isolated neurons. They are slow/fast systems, where a slow subsystem

100 drives the fast subsystem between different states. In such models, the studied fast subsystem

101 delineates the neuronal membrane electrophysiological activities. The slow subsystem can be

102 represented by variations of different slow variables including ion concentration (Barreto and

103 Cressman 2011; Chizhov et al. 2018; Cressman et al. 2009; Hübel and Dahlem 2014; Kager

104 et al. 2000; Øyehaug et al. 2012; Y Wei et al. 2014; Yina Wei, Ullah, Ingram, et al. 2014),

105 oxygen level (Yina Wei, Ullah, and Schiff 2014; Yina Wei, Ullah, Ingram, et al. 2014), volume

106 (Øyehaug et al. 2012; Y Wei et al. 2014) and interaction with glial cells (Hübel and Dahlem

107 2014; Øyehaug et al. 2012). These models provide mechanistic insights, in particular how the

108 slow variable influences neuronal activity, including the transitions from "healthy" regimes to

109 "pathological" ones like SLEs and DB. However, none of these models, including the

110 extracellular slow variations, could be reduced to four variables, while presenting a bursting

4

111   pattern corresponding to the most common ones encountered at the network level, i.e. the

112   SN/homoclinic pair (Jirsa et al. 2014). The reduction of a model to a small number of

113   dimensions while maintaining the link with physical quantities, makes it possible to establish a

114   direct link between biophysics and a simple dynamical description. Since SLEs, SIA and DB

115   pertain to the dynamic repertoire of The Epileptor and of biological neuronal networks (El

116   Houssaini et al. 2015; Saggio et al. 2017), biophysical models should be able to reproduce all

117   three types of activities. The goal of the present study is to identify candidate mechanisms from

118   physiology robustly leading to the time scale separation and trajectories in SLEs. We will take

119   guidance from the careful dynamic analyses performed in previous works.

120   In generic models, the dynamics is well understood (Jirsa et al. 2014; Saggio et al. 2017) but

121   these models rarely offer direct biophysical insight as they use abstract parameters. Important

122   works have been done to understand the link between phenomenological and biophysical

123   models (Bernard et al. 2014; Naze et al. 2015). In order to explore the dynamics repertoire,

124   the high dimensionality of detailed biophysical models must be reduced. A minimal model of

125   interictal and SLEs has been introduced as Epileptor-2, using increase in $[K]_o$ to trigger burst

126   discharges and restoration of the K^+ gradient via the sodium-potassium pump to stop SLEs

127   (Chizhov et al. 2018). The work of Saggio et al. (Saggio et al. 2017) is a generalization of the

128   dynamics found in Epileptor and Epileptor-2. However, Epileptor-2 does not produce the

129   SN/homoclinic bifurcation consistently found experimentally, and the model does not generate

130   SIA or DB. Moreover, when the fast discharges stop, the slow variables of Epileptor-2 continue

131   oscillating, whereas that of Epileptor 1 do not. This can be understood on the basis of the

132   results of Saggio et al.(Saggio et al. 2017). In the present reduction, we used a Hodgkin-

133   Huxley-like single cell model, and we imposed several constraints: SLE, SIA and DB (El

134   Houssaini et al. 2015), as well as the SN/homoclinic bifurcation must be present. We have thus

135   generated a reduced slow/fast system preserving biophysical representation and satisfying

136   these constraints. A variable acting on a slow time scale is necessary to drive the system

137   through different activities (e.g. from SLE to DB). In a cell, numerous processes can occur on

5

138   a slow time scale and act as a slow variable, including changes in ion concentration,

139   metabolism, phosphorylation levels, and transcription. Ion homeostasis regulation is critical to

140   maintaining neuron function, and many sub-cellular mechanisms are involved in this process

141   (Dubyak 2004). Fluctuations of ion concentrations in the extracellular space modulate the

142   electrophysiological activity of a single neuron (Cressman et al. 2009; Yina Wei, Ullah, and

143   Schiff 2014). The present work focuses on extracellular potassium ($[K]_o$) concentration

144   because it increases during seizures (de Curtis et al. 2018; Fisher et al. 1976; Fröhlich et al.

145   2008; Lux et al. 1986; L. Wang et al. 2016), even in the absence of synaptic activities (de

146   Almeida et al. 2008; Jefferys and Haas 1982). Augmentation of $[K]_o$ is also observed in head

147   injury (Katayama et al. 1990; Reinert et al. 2000), which can be a starting point for epilepsy

148   (Lowenstein 2009). Computational simulations show that potassium could be responsible for

149   local synchronization (Durand et al. 2010) and is an important parameter in neural dynamics

150   (Barreto and Cressman 2011; Cressman et al. 2009; Ullah and Schiff 2010; Yina Wei, Ullah,

151   and Schiff 2014). In addition, in experimental models, the transition to DB correlates with a

152   much larger increase of $[K]_o$ as compared to SLEs (El Houssaini et al. 2015; Gloveli et al.

153   1995). We here consider the slow modulatory effects of $[K]_o$ variations. In our model, the slow

154   sub-system describes ionic concentration variations. The fast subsystem characterizes the

155   dynamics of trans-membrane ion flows through voltage-gated and the sodium-potassium

156   pump, and so allows tracing the membrane potential. We report that this single cell model

157   accounts for the SN/homoclinic bifurcation pair and that it reproduces SLEs, SIA and DB,

158   reproducing patterns found in single neurons recorded experimentally during seizures.

Results

160   Our goal was to construct a biophysical model at single neuron level that can reproduce

161   the different firing patterns recorded when extracellular potassium is experimentally increased,

162   while keeping it sufficiently simple to allow a bifurcation analysis. The model is schematized in

163   Fig.1 (see methods section for the equations). It is a simplification of the classical Hodgkin-

164   Huxley formalism, which also includes close surrounding environment thanks to a description

165   of three compartments (external bath, extracellular space, intracellular space).
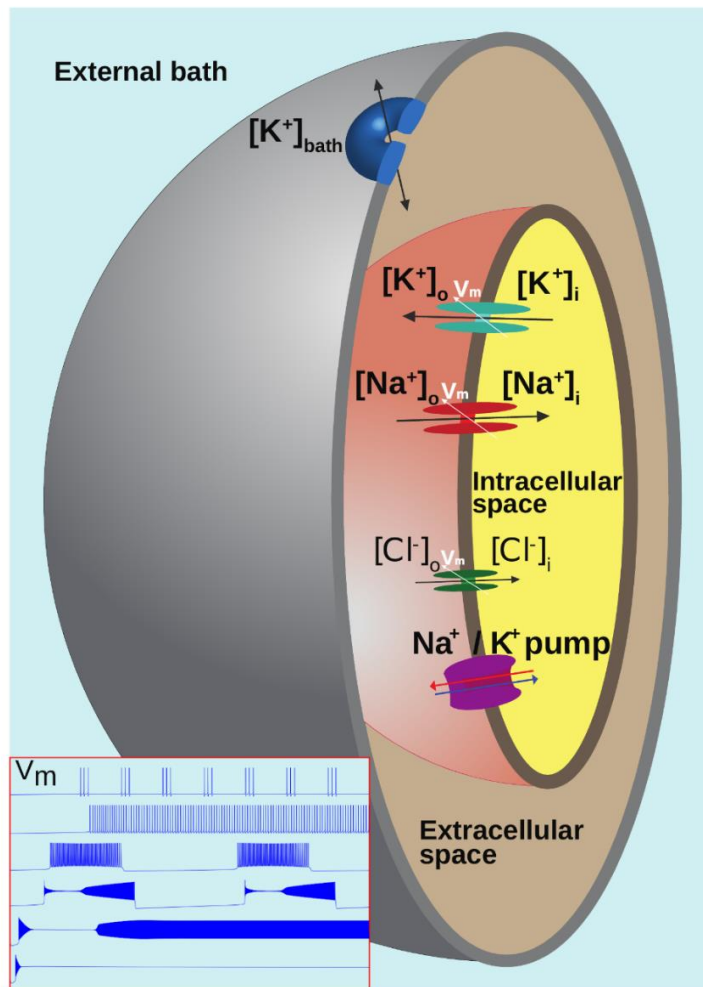

183   **Figure 1: Diagram of characteristics and mechanisms described by the model.** Three
184   compartments are represented. A passive diffusion of potassium exists between the external
185   bath and the extracellular space. Na^+, K^+ and Cl^- ions can be exchanged between the
186   extracellular and intracellular compartments via the Na/K-pump and voltage-gated channels.
187   This model can reproduce the typical patterns of the membrane potential V_m, shown in the
188   bottom left subplot, including tonic firing, bursting, seizure like events (SLE), sustained ictal
189   activity (SIA) and depolarization block (DB).

190

191   Numerous experiments show that seizures and SLEs are associated with an increase

192   in $[K]_o$ (Fisher et al. 1976; Fröhlich et al. 2008) and that increasing of external [K] can trigger

193   SLEs (S. F. Traynelis and Dingledine 1988; Stephen F. Traynelis and Dingledine 1989). The

194   model presented here takes into account the regulation of potassium, via the possible diffusion

195   towards the external bath compartment and its associated potassium concentration $[K]_{bath}$.

7

196   Changing $[K]_{bath}$ parameter will strongly influence the regulation of extracellular potassium by

197   allowing or not the removal of excess potassium from the extracellular compartment. When

198    $[K]_{bath}$ is low, the bath compartment can pump out the extracellular potassium; but it fails to do

199   so when it is saturated by potassium. We thus explored the response of the model as the

200   concentration of $[K]_{bath}$ was increased. The gradual increase in potassium led to 7 sequential

201   qualitative firing patterns: Resting State (RS), Spike Train (ST), Tonic Spiking (TS), Bursting,

202   Seizure-like events (SLE), Sustained Ictal Activity (SIA), and Depolarization Block (DB) (Note

203   that what is called here Spike Train also corresponds to another type of burster from a

204   dynamical point of view (E. Izhikevich 2007; Saggio et al. 2017)). The corresponding changes

205   of membrane potential for all these patterns are shown in Fig.2.

206   The number of firing patterns is higher than in the original Hodgkin-Huxley model. This

207   is due to the fact that the model takes into account the variations of concentration, as

208   evidenced by the variation of the Nernst potentials. The changes in Nernst potentials for

209   sodium and potassium ion species are shown in Fig.2. The simulations are initialized with

210   values observed in a "healthy" resting situation, it is therefore possible to observe the transition

211   linked to the increase in the parameter $[K]_{bath}$. In some cases, the Nernst potentials display a

212   transient change before reaching a sustain low amplitude oscillations following action

213   potentials, as observed during RS, TS, SIA and DB. During periodic events, (ST, Bursting,

214   SLE), larger oscillations are observed in Nernst potentials. These oscillations are directly linked

215   to the observed oscillations in the slow variables of the model (Eq.(3) and Eq.(4)) describing

216   concentration changes. The rate of oscillation of the slow variables thus explain the duration

217   of periodic events, in line with the assumed essential role of ionic homeostatic regulation.

218   Each of the firing patterns can be associated to a different behavior, observable

219   experimentally at different scales. The correspondence is established on the basis of their

220   shape and their order of appearance as $[K]_{bath}$ is increased. Tonic and bursting patterns are

221   prototypical. We consider the activity shown on Fig. 2d as SLE at the neuronal scale, as it is

222   similar to the activity typically recorded in individual neurons (Haglund and Schwartzkroin

223 1990), in particular the transient episode of depolarization block, in different experimental

224 preparations during SLEs at the network scale (e.g. Fig. 6 in (Uva et al. 2013); Fig. 1 in (Bikson

225 et al. 2003) or Fig. 8 in (Jirsa et al. 2014)). Although it is possible to generate SIA *in vitro*

226 (Quilichini et al. 2002), the corresponding intracellular activity is not known, however the

227 sustained firing pattern in the model cell resembles the regular field activity recorded during

228 status epilepticus like events *in vitro* (Quilichini et al. 2002). The sustained DB at the single cell

229 level corresponds to what is observed experimentally during network spreading depolarization

230 when $[K]_o$ reaches high levels (G G Somjen 2001).

231   Increasing $[K]_{bath}$ leads to different regimes of variation of external potassium (Fig.3).

232 These different regimes are associated with a specific dynamic (i.e. type of bifurcation) of the

233 excitability of the membrane. It is therefore possible to link the membrane potential to the

234 variations in extracellular potassium, because of exchanges existing between compartments

235 (i.e. via the slow variable), as shown in Fig.4. In the next subsection, we detailed these

236 dynamical interactions for the different patterns of activity, following the order of appearance

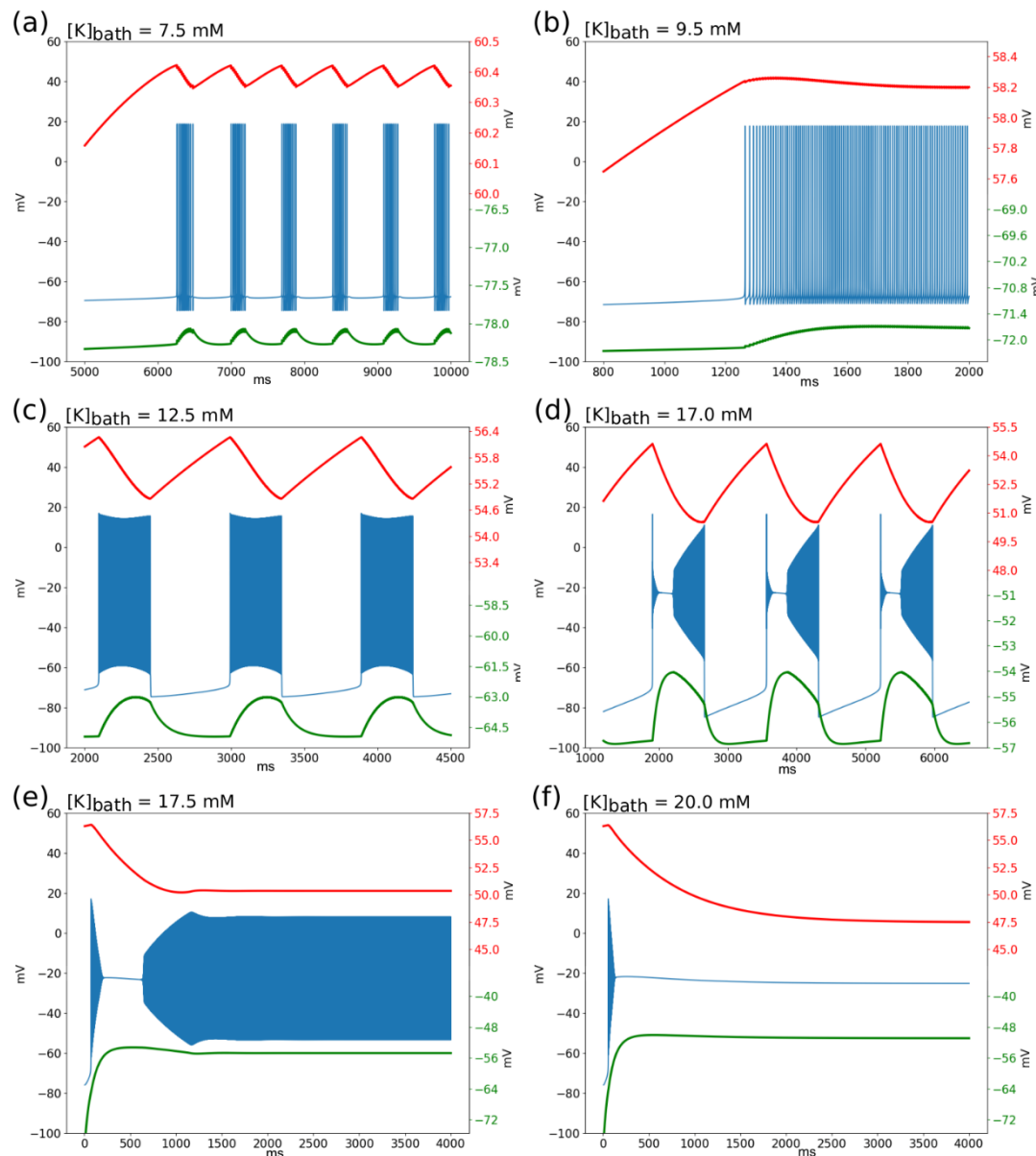237 when $[K]_{bath}$ increase.

238

239

240

241

242

243

244

Figure 2: qualitative mode of behavior of the membrane potential and Nernst potentials.
In blue: time series of the membrane potential V_m for the following patterns of activity: (a) Spike train, (b) Tonic spiking (TS), (c) Bursting, (d) Seizure-like event (SLE), (e) sustained ictal activity, (f) Depolarization Block (DB). In red: Nernst potential of sodium, in green: Nernst potential of potassium with specific Y axis on the right side. If the value of $[K]_{bath}$ stays below 6 mM, the system remains in resting state around -72 mV. Specific patterns of activities start to appear with a diminution of the Nernst potential of sodium and an increase of the Nernst potential of potassium. When periodic events are occurring (panels c and d), oscillations can also be observed in the Nernst potential of both ions.

254

255

256

257 **Resting states, spike train and tonic spiking in low [K]$_{bath}$**

258   Resting state is found when [K]$_{bath}$ is around the normal value of [K]$_o$ (called [K]$_{0,o}$, see

259 Methods section). If [K]$_{bath}$ is smaller than [K]$_{0,o}$ the membrane potential slowly hyperpolarizes,

260 due to a diffusion of potassium in the direction of the external bath. When [K]$_{bath}$ slightly

261 increases (> 7 mM), ST appears through a SNIC bifurcation. The offset is also a SNIC

262 bifurcation. In this case, the onset and offset bifurcations can be easily identified by their

263 characteristic features (Saggio et al. 2017), and confirmed by numerical methods (using

264 SymPy (Meurer et al. 2017) and SciPy (Millman and Aivazis 2011) libraries). With higher value

265 of [K]$_{bath}$ (> 8 mM), TS occurs. In this condition, [K]$_o$ stabilizes (Fig.3), and the neuron fires at a

266 constant frequency (Fig. 2b). The occurrence of regular spiking due to an increase of [K]$_o$

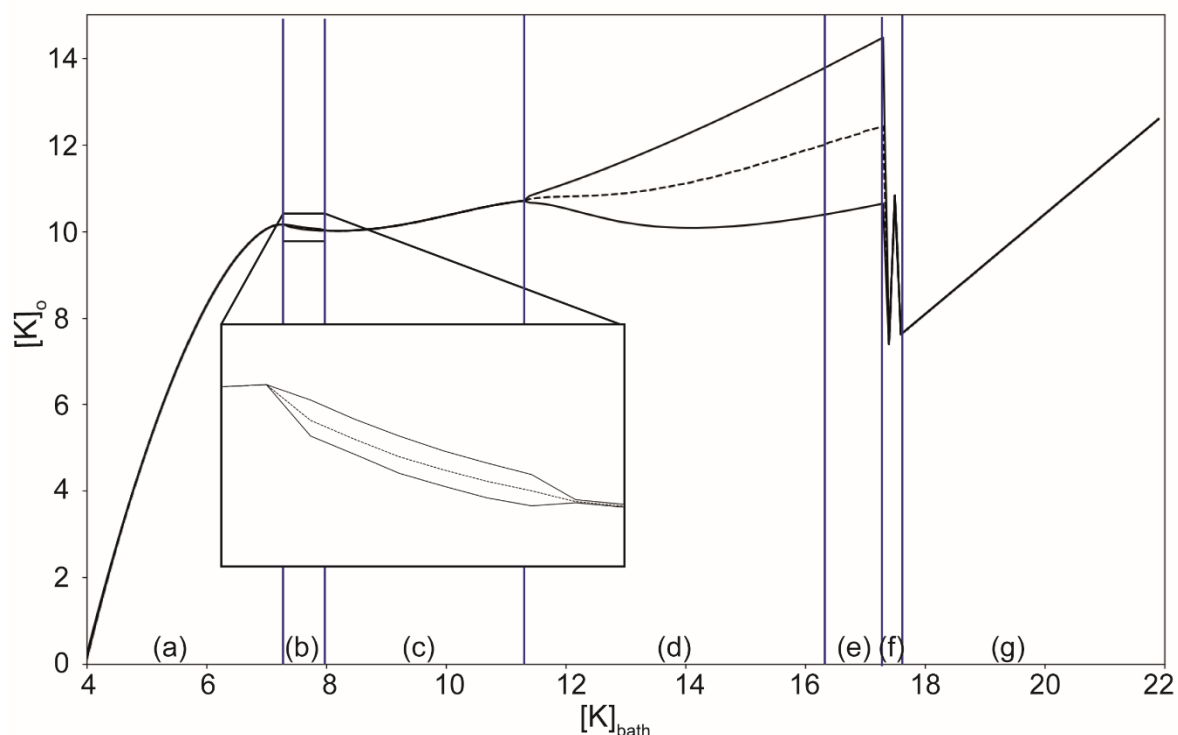267 through diffusion from the bath is consistent with experiments [29].

268 **Figure 3: Variation of extracellular potassium concentration as a function of [K]$_{bath}$.**
269 Minimal and maximal external potassium [K]$_o$ and mean (dash line) concentration observed
270 during simulations done for different values of the parameter [K]$_{bath}$. Due to diffusion from the
271 external bath, increasing [K]$_{bath}$ leads to variations in [K]$_o$. Different patterns are observed for
272 each range of [K]$_{bath}$: (a) resting state, (b) spike train, (c) regular spiking, (d) burst, (e) seizure
273 like event, (f) sustained ictal activity, (g) depolarization block. The periodic events (spike train,
274 burst and seizure-like event) correspond to the range of [K]$_{bath}$ where [K]$_o$ periodically oscillates.

275

11

276 **Bursting and Seizure-like events**

277   Bi-stable behavior occurs when the slow system starts to oscillate when $[K]_{bath}$ is further

278 increased. The model (with parameters listed in Table 1) displays bursting and SLE,

279 successively. Bursts are square-wave bursts (SN/Homoclinic bifurcations) and SLEs also

280 show SN and Homoclinic bifurcations at onset and offset, respectively (See supplementary

281 information: S1, S2, S3, S4). Here, the slow subsystem oscillates in a self-sustained manner

282 (Fig. 4a-f), generating recurrent bursting or SLEs, with important variations of $[K]_o$, due to

283 oscillations in the slow subsystem. The combined effects of oscillations of $\Delta[K]_l$ and $[K]_g$ explain

284 the changes in the Nernst potential of potassium (and sodium, which is linked to potassium in

285 the model), thus changing neural excitability. During spiking activity, voltage-gated potassium

286 channels open increasing potassium current I_K. The influence of I_K in the equation of $\Delta[K]_l$

287 (eq.3), explains the decrease of $\Delta[K]_l$, hence the increase of $[K]_o$ through equations (eq.16) and

288 (eq.20). This is consistent with the observations described in (Fisher et al. 1976). The increase

289 in $[K]_o$ starts with the occurrence of burst and SLEs. Thus, it is not the cause of the event but

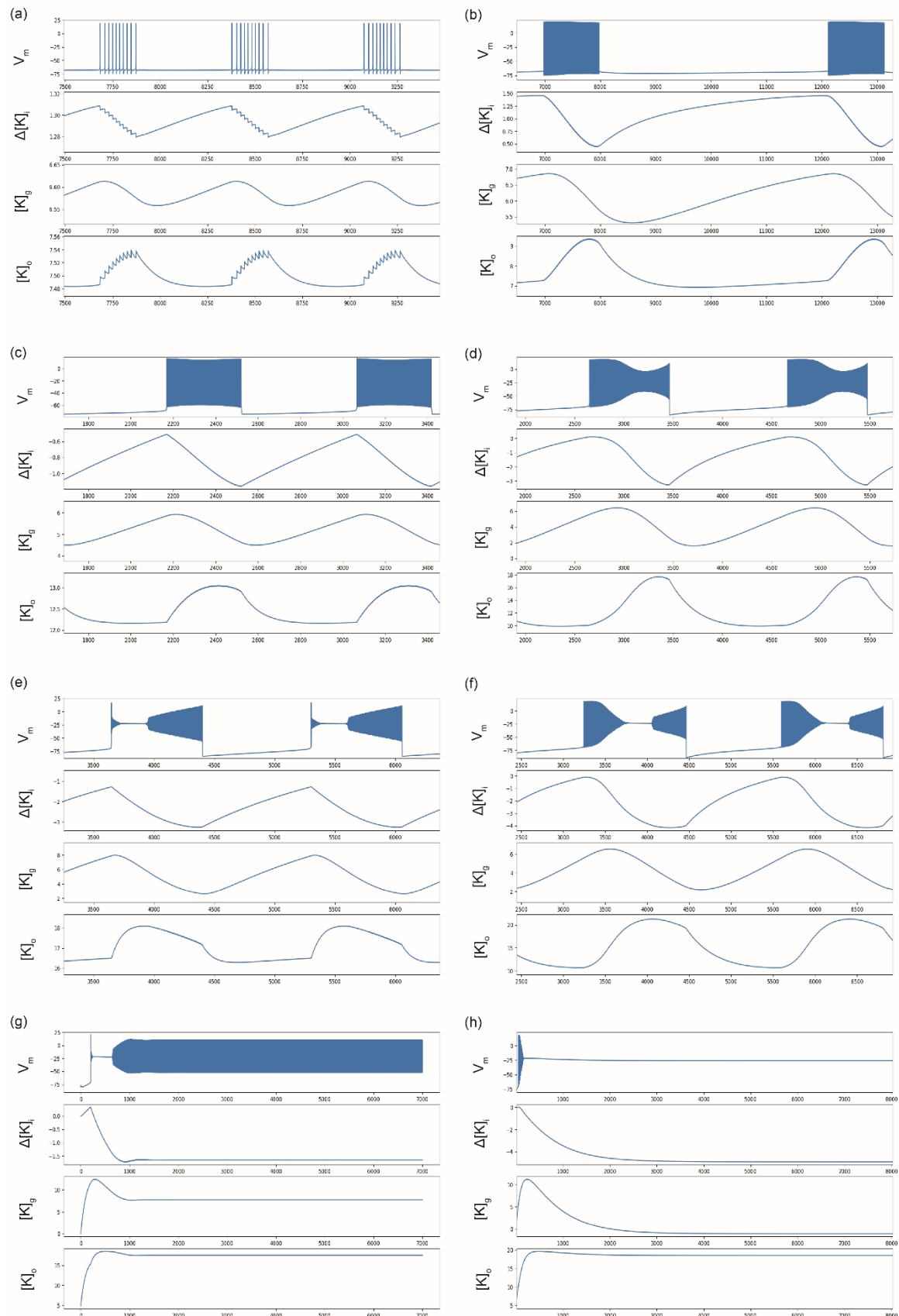290 a consequence of homeostasis dysregulation (i.e. augmentation of $[K]_{bath}$).

291

13

Figure 4: Time series of membrane potential, Δ[K]$_i$, [K]$_g$, and [K]$_o$. obtained thanks to numerical methods using SciPy library (Millman and Aivazis 2011), x-axis in millisecond. (a) spike train with [K]$_{bath}$ = 7.5 mM, (b) spike train with [K]$_{bath}$ = 7.5 mM and γ = 0.04, ε = 0.002, (c) Burst with [K]$_{bath}$ = 12.5 mM, (d) Burst with [K]$_{bath}$ = 12.5 mM, and γ = 0.06, ε = 0.002, (e) SLE with [K]$_{bath}$ = 16 mM, (f) SLE with [K]$_{bath}$ = 16 mM and γ = 0.08, ε = 0.0008, (g) SIA with [K]$_{bath}$ = 17.5 mM, (h) DB with [K]$_{bath}$ = 20 mM. If not specified, the parameter values used here are the reference parameters described in the method section. Variations of Δ[K]$_l$ and [K]$_g$ induce different patterns of activity. The combined effects lead to the observed variations in [K]$_o$. The time scale of the slow variables γ and ε influence the shape of V$_m$ allowing the system to exhibit SN or SNIC bifurcation at the onset of the events.

Steady states, SIA events and DB, in high [K]$_{bath}$ conditions

SIA events (Fig. 2g) appears for [K]$_{bath}$ around 17.5 mM (Figs. 3 & 4), i.e. above the threshold value for SLEs as reported experimentally (El Houssaini et al. 2015). If no other mechanisms act to stop it, these oscillations remain constant (analogous to refractory status epilepticus). Permanent DB occurs for even higher values of [K]$_{bath}$ (> 18.0 mM, Fig. 3) as also reported experimentally (El Houssaini et al. 2015). In these cases, after a peak value (Fig. 4h), [K]$_o$ stabilizes, explaining the short range of variation (Fig. 3). These steady-states start like a SLEs (Fig. 4e-f), then the slow variables stabilize and [K]$_o$ remains constant at a high value (Figs. 4g-h).

We conclude that the model behaves as expected from the biological observations, when experimentally increasing of [K]$_{bath}$. These simulations were obtained when using a "healthy" situation, i.e. as if recording a "control" neuron. In the next section, we model a "pathological" situation for which where the regulatory mechanisms of neuronal homeostasis are affected.

Influence of other parameters

We then aimed to identify relevant parameters that could describe "healthy" and "pathological" states. Experimental data show that impairment in potassium buffering by glial cells leads to pathological behavior (Coulter and Steinhäuser 2015; Hubbard and Binder n.d.; Rangroo Thrane et al. 2013; Scholl et al. 2009). Three model parameters correspond to homeostasis regulation, involving two mechanisms: the ion exchange capacity between

14

323   compartments (ε and γ parameters in the model), and the maximum capacity of the Na/K pump

324   (ρ in the model). A variation of ε corresponds to a degradation of the interaction with glial cells

325   (Coulter and Steinhäuser 2015; Kofuji and Newman 2004; Olsen et al. 2015; Walz 2000) which

326   normally ensures the regulation of the extracellular concentration of K^+. Homeostasis of

327   intracellular ions is also critical, and a variation of γ corresponds to an impairment of such

328   mechanisms, not detailed in this model, such as co-transporters and exchangers (Hille 2001;

329   Kandel, Eric R., Schwartz James H., Jessell Thomas M. n.d.). Changes in both parameters

330   can also be considered. In the model, they are equivalent to a change in volume while keeping

331   the β ratio constant. Varying the time constants of the slow subsystem (ε and γ), leads to

332   different bi-stable behaviors. Two examples are shown in Fig. 4, (b) with γ = 0.04, ε= 0.002,

333   (d) γ = 0.06, ε = 0.002, and (f) γ = 0.08, ε = 0.0008, in these situations the shape of the

334   oscillations of potassium concentration are affected leading to a change in the duration of the

335   events. For burst and SLE shown in Fig4. d and f, the model exhibits a different class of onset

336   bifurcation. For both, a saddle-node on invariant cycle (SNIC) bifurcation at the onset and

337   homoclinic bifurcation at the offset can be identified, thanks to their specific dynamics and

338   resulting shapes (E. Izhikevich 2007; Saggio et al. 2017).

339   The other key parameter to consider is the pump rate ρ. The Na/K-ATPase is described

340   by Eq. (8) in the model. In a biological neuron, the pump depends on ATP and during status

341   epilepticus, the ATP concentration augments due to high needs and then decreases (Lietsche

342   et al. 2016). The ATP concentration is not taken into account in the model, but the maximal

343   Na/K-pump rate is modulated by the parameter ρ. This parameter also influences the shape

344   of I_{pump} response as a function of $[Na]_i$ and $[K]_o$ (Fig.5a). For large values of ρ, the pump is

345   activated for lower value of $[Na]_i$ and $[K]_o$ (Fig. 5a). We find that burst duration changes with ρ

346   for a fixed $[K]_{bath}$ (Fig. 5b), where a faster activation (higher ρ) leads to shorter bursts. The

347   augmentation of ρ does not necessary lead to an increase of I_{pump}; it affects the general

348   dynamics of the whole system (Fig. 5c).

349

350
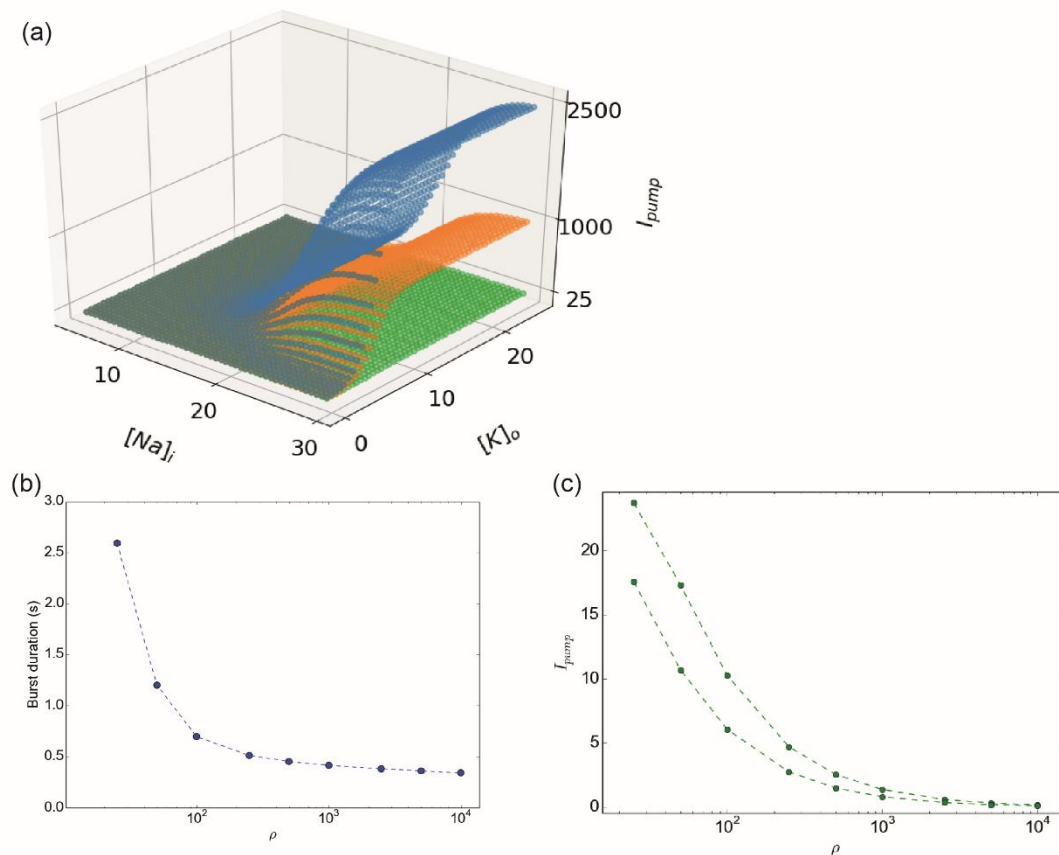
Figure 5: Influence of the activity of the Na/K-pump. (a) I_{pump} function for ρ= 25 (green), ρ= 1000 (orange), ρ= 2500 (blue). The initial slope when the system moves away from the concentrations at rest is affected, explaining the modification of the influence of I_{pump} in the dynamic of the system. (b) Burst duration as a function of ρ for $[K]_{bath}$ = 14.0 mM. Bursts have shorter durations for higher value of ρ. (c) Minimal and maximal pump current, I_{pump}, observed during simulation done with $[K]_{bath}$ = 14.0 mM. The range of I_{pump} decreases for higher ρ values.

357

All these observations show that the model presents a behavior consistent with experimental

observations. Importantly, the biophysical model is able to reproduce general patterns of

activities (i.e. periodic events) as generated by the phenomenological model (El Houssaini et

al. 2015). Phenomenological models, which present a minimal number of variables and

parameters, allow an exhaustive study of the dynamics. The biophysical model used here

contains too many parameters for an exhaustive study of the dynamics, but reducing the

364   number of variables will allow a comparison with the generic model. In the next section, we

365   analyze the dynamics of the model.

366   **Dynamical observations**

367   The model can be divided into the fast (V, n, respectively Eq.1 and Eq.2) and the slow

368   subsystems ($\Delta[K]_i$, $[K]_g$, respectively Eq.3 and Eq.3). The slow system can oscillate and drive

369   the fast system between different behaviors, in particular switching between resting state and

370   fast oscillations to obtain bursting-like activity. This type of phenomenon, corresponding to slow

371   fast systems, has been extensively studied from a theoretical point of view, in particular for

372   neural activity (E. Izhikevich 2007; Saggio et al. 2017). In this subsection, to allow a better

373   correspondence with the theoretical framework, we call burster a system allowing these

374   periodic events. To create the oscillation in the slow subsystem, theoretical works show that

375   two mechanisms are possible (E. Izhikevich 2007; Saggio et al. 2017): Slow-Wave (SW)

376   burster, where the slow subsystem is made of two equations, independent of the fast system,

377   or Hysteresis-Loop (HL) burster where the slow subsystem is made of only one equation that

378   depends on the fast system. Each has typical onset/offset bifurcation pairs. These specific

379   paths for bursting have been identified in the generic model (Saggio et al. 2017), and are

380   reproduced in fig.6a. We first verified if the relations between the equations of the slow and

381   fast systems allow the existence of the mechanisms described previously. In our model, two

382   equations describe the slow subsystem (Eq.(3), (4)). Because I_K (Eq.(6)) depends on V and n,

383   the Eq.(3), depends on the fast system. This corresponds to a relation that exists in an HL

384   burster. The second equation of the slow subsystem, Eq.(4), also depends on the Eq.(3),

385   through the Eq. (20). Thus, there exists a relation between the two equations of the slow

386   system, enabling oscillation such as in a SW burster. These relations between the variables of

387   our model allow obtaining the two types of bursters previously described.

388   We therefore tested for possible correspondences between our model and the generic

389   model. We were able to identify the regions in the generic model capturing the dynamics

390   reproduced by our model in Fig.6a. The center of the region of interest has been marked with

17

391 a yellow star in fig. 6a. for the generic model and its correspondence in the bifurcation diagram

392 of our model in Fig. 6b. In this bifurcation diagram we show two possible paths of our model,

393 for burst behavior (Fig. 6b, top) and for SLE (Fig. 6b, bottom). It crosses regions of stable

394 resting state (in white), depolarized (red), and bistable (light red). It is therefore possible to

395 establish a non-exhaustive list of the correspondences between the paths of the two models.

396 The paths for the periodic events have been listed in Fig. 6c. The spike train, Bursting and SLE

397 behaviors correspond to paths, $c5$, $c2$ and $c10$, respectively. The bursting behavior with

398 changes in ε and γ (Fig. 4b) that represents the SNIC/SH bifurcation corresponds to the path

399 $c6$. The model proposed here, consistent with biophysics, fits into the framework of the generic
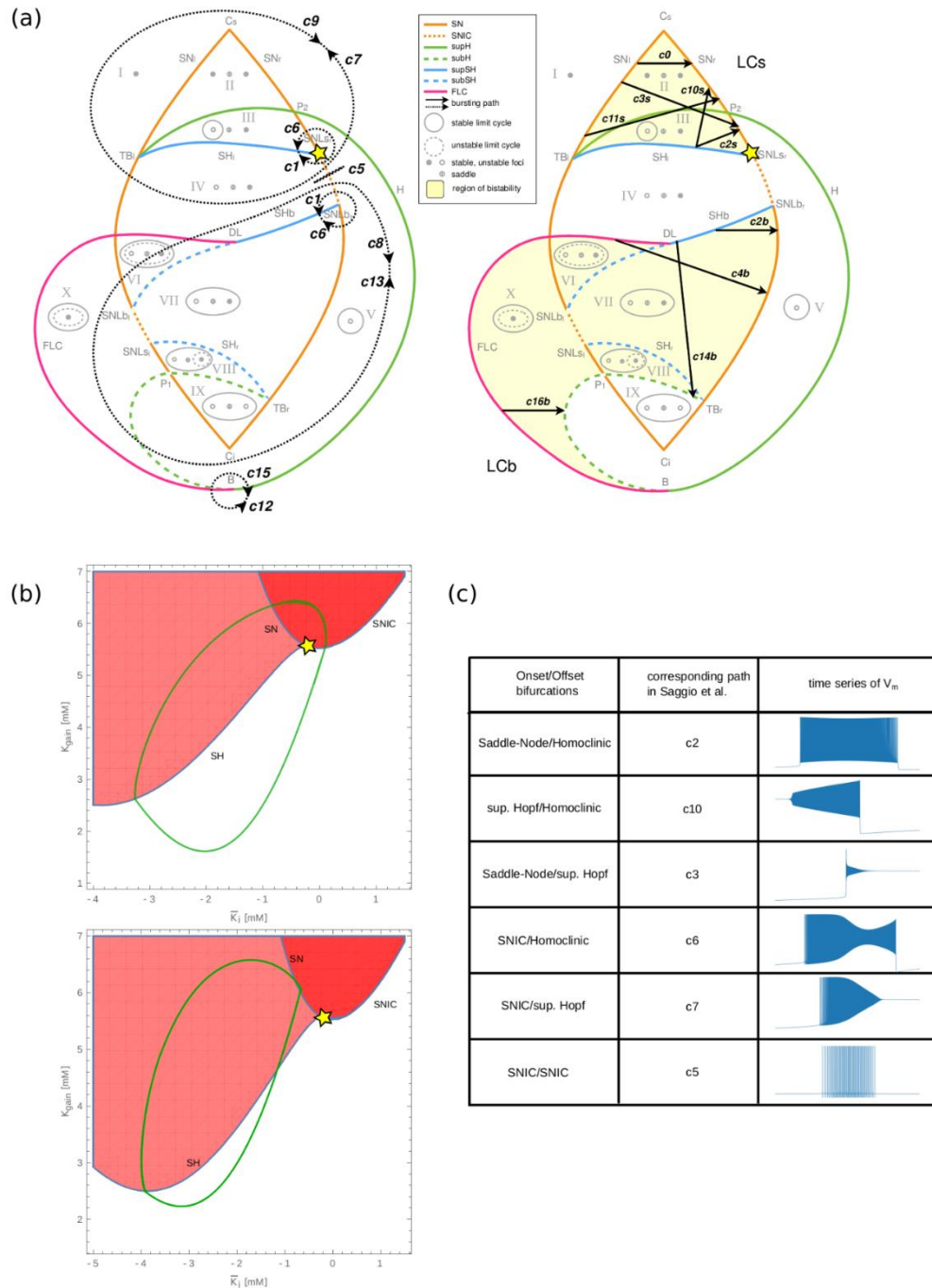
400 model.

Figure 6: Comparison with the generic model. (a) Paths for bursting activity of the generic model proposed by Saggio et al. adapted with authorization from (Saggio et al. 2017), for hysteresis-loop burster (left) and slow-wave burster (right), the yellow star corresponds to the center of the region captured by our model. (b) Bifurcation diagram of our model, where the white area corresponds to 'resting state only' region, the dark red corresponds to a depolarized region, and the light-red region is the region of bi-stability. The yellow star corresponds to the point also found in the generic model, where the SH, SNIC and SN bifurcations intersect. In the top diagram, the green line corresponds to the path taken by the burster, in the bottom one to the path taken by the SLE. (c) Classes of bursters found in the model, and the corresponding path in the generic model.

412   Since our biophysical model reproduces the bifurcations of the generic model for

413   different types of network activities, it becomes possible to investigate the ionic mechanisms

414   underlying the onset/offset bifurcations. The fast subsystem can be described fixing all

415   parameters (tables 1 and 2) and considering the two slow variables as parameters. Fixed

416   points can thus be found for different values of $\Delta[K]_i$ and $[K]_g$ as shown in Fig. 7. Importantly,

417   some parameter values allow a bi-stable behavior. It is thus possible to understand the direct

418   relationship between the biophysical variations in potassium concentration and the type of

419   bifurcations by observing the trajectory of the membrane potential in this space for periodic

420   events identified previously. During periodic oscillatory behavior, the neuron is initially in

421   resting state (blue plane). The membrane potential slowly increases due to the rise in

422   extracellular potassium, until it reaches a SN (green plane) and then encounters a limit cycle.

423   The slow subsystem then drives it to a negative value of $\Delta[K]_i$, were the limit cycle meets a SN

424   producing homoclinic bifurcation. These bifurcations are observed at the onset and offset of

425   bursting and SLE behaviors in the model. To have a better understanding of these trajectories,

426   animations with the dynamics of the fast subsystem are available in supplementary material

427   (Fig. S1, S2, S3, S4). We therefore have here a means of bringing together the biophysical

428   aspects, described previously, with the phenomenological vision of dynamical systems
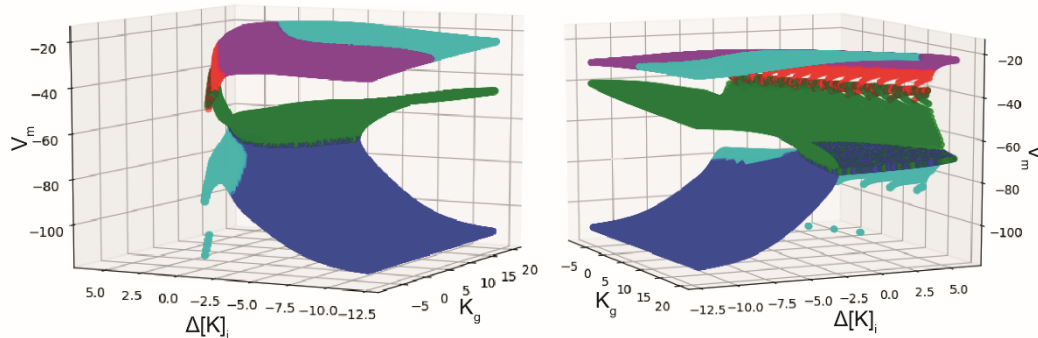
429   approach.

430

Figure 7: Fixed points of the fast subsystem. Fixed point of the fast subsystem (V_m) considering the variables from the slow subsystem as parameters. We used a numerical methods with SymPy (Meurer et al. 2017) and SciPy (Millman and Aivazis 2011) libraries, to find the roots and the eigenvalues of the Jacobians of the 2D fast subsystem, and thus the stability considering the existence and the sign of real and imaginary parts of the eigenvalues of the Jacobians. Blue: stable node, green: saddle node, cyan: stable focus, magenta: unstable focus, red: unstable node. Two different angles of view are presented, illustrating the manifold that permits bi-stability.

Discussion

The aim of this work is to develop a minimal biophysical model at single neuron level based on time scale separation, where the system is able reproduce the dynamics which have been identified in experiments (Bikson et al. 2003; Jirsa et al. 2014; Quilichini et al. 2002; George G. Somjen 2001; Uva et al. 2013) and described by generic models (Jirsa et al. 2014; Saggio et al. 2017) . For this purpose, we developed a three-compartment model: a cell equipped with voltage-gated channels to generate action potentials, and Na+/K+ pump to maintain stable ion concentration, an extracellular space surrounding the cell and an external bath that can uptake/release potassium from/to extracellular space. We managed to describe the interaction between these compartments using a system of four differential equations describing two fast and two slow variables. The fast variables delineate excitability while the slow ones, outline potassium changes from the first and third compartments. The sodium concentration changes are not excluded from our model but are linked to potassium through the electroneutrality principle. We have shown that despite its simplicity the model was able to

21

454   mimic six electrophysiological behaviors classically recorded in neurons and neuronal

455   networks, via the variation of only one parameter. All parameter values were within biophysical

456   ranges (Table1) (Hille 2001; Kandel, Eric R., Schwartz James H., Jessell Thomas M. n.d.).

457   The model has two main limitations. The fast system describes only intrinsic excitability and

458   does not include synaptic currents. And, the slow system is based (only) on potassium

459   concentration. Introducing synaptic inputs would increase the dimension of the system. We

460   propose that synaptic inputs would act as a noise generator increasing the probability to reach

461   the bifurcation as demonstrated experimentally (Jirsa et al. 2014); including them should not

462   change the general behavior of the model. Furthermore, ion homeostasis is not reduced solely

463   to potassium. Potassium is just one candidate among many others for the slow system.

464   Numerous studies have reported large changes in concentration of Ca^{2+} (Heinemann et al.

465   1986), Cl^{-} (Miles et al. 2012; Raimondo et al. 2015) and neurotransmitters during seizures

466   (Chapman et al. 1984; During and Spencer 1993). Likewise, decreasing extracellular Ca^{2+}

467   leads to seizures (Jefferys and Haas 1982), which are characterized by SN/homoclinic

468   bifurcations (Jirsa et al. 2014). Since it is possible to trigger similar SLEs via totally different

469   biophysical mechanisms (Jirsa et al. 2014), we propose that the K^{+}-dependent mechanism we

470   describe, is one among many the possible paths leading to the same end point. In our model,

471   changes in potassium constitute the causal factor driving the neuron through different types of

472   activities. Although similar changes in potassium are measured experimentally when networks

473   (and not cells) undergo such transitions, causality has not been demonstrated experimentally,

474   only correlation. Another limitation exists due to the formalism used. If $[K]_{bath}$ tends to zero then

475   membrane potential hyperpolarize until the Nernst potential are no longer defined due to

476   division by zero. We reach here the limit of the conductance-based model from Hodgkin-

477   Huxley formalism. Due to the expression of the Nernst potential, if the ratio $[K]_{o}/[K]_{i}$ approaches

478   zero, then the I_K current increases towards infinity, which is not physiologically plausible.

479   Another factor to consider is that the dynamics of the single cell is driven by slow changes of

480   extracellular variables, which, in a biological system, is shared with neighboring cells. So, these

481   slow variables can also be responsible for the genesis of network activity (Naze et al. 2015).

22

482   As these mechanisms exist both at the network and single neuron level, it would be simplistic

483   to conclude that a seizure at the network level is due to the combined expression of seizures

484   at the single cell level. Since a neuronal network can be seen as a complex system of many

485   components, coupled in a non-linear manner, seizures may just be an emergent property,

486   perhaps taking advantage of the fact that they are already encoded at the single cell level. The

487   same consideration applies to other pathological activities such as SIA and DB, which

488   corresponding pattern have been found in dynamics of our model.

489   However, we only studied the dynamics for variations of few chosen parameters based

490   on physiological observations identified in previous works. The parameters explored here show

491   that the model can produce different combinations of onset/offset bifurcations. Numerous

492   studies used ion concentration variations in biophysical models to generate various types of

493   activity (Barreto and Cressman 2011; Bernard et al. 2014; Cressman et al. 2009; Florence et

494   al. 2009; Krishnan et al. 2015; Øyehaug et al. 2012; Yina Wei, Ullah, and Schiff 2014; Yina

495   Wei, Ullah, Ingram, et al. 2014). Descriptions of ion concentration dynamics for bursting have

496   been done by Barreto *et al.* (Barreto and Cressman 2011), based on a slow/fast system. In

497   this work, the bifurcations for SLEs are SNIC and Hopf. This approach, based on ion

498   concentration dynamics, permits the unification of spike, seizure and spreading depression

499   proposed by Wei and al. (Y Wei et al. 2014). As different models can lead to similar dynamics

500   (Prinz et al. 2004), this may suggest that different minimalist models are possible to obtain a

501   unified framework. In our work, we proposed a conductance-based model of the neuronal

502   membrane, exhibiting an extended repertoire of behavior and introducing sustained ictal

503   activity in a unified framework. Another difference with previous work is that our model can

504   exhibit bi-stable modes saddle-node/homoclinic bifurcations, which are the most commonly

505   observed in recordings from patients and experimental animal models (Jirsa et al. 2014). Our

506   model does not take into account variation of volume or oxygen homeostasis as in (Y Wei et

507   al. 2014) but, only variations of ion concentrations, driven by diffusion of potassium from EB.

508   It seems intuitive that other biological variables could be considered as slow variables to drive

23

509 the fast subsystem in a reduced biophysical model. The work of Øyehaug*et al.*(Øyehaug et al.

510 2012) presents interesting dynamical features with saddle-node/homoclinic bifurcations for

511 SLEs. However, this model is much more complex as it describes numerous biological features

512 and mechanisms. In comparison to previous works (Barreto and Cressman 2011; Krishnan et

513 al. 2015; Øyehaug et al. 2012; Yina Wei, Ullah, Ingram, et al. 2014), our model is reduced to

514 only four equations. We sought to include only a minimal number of mechanisms necessary

515 to reproduce neural dynamics. Chizhov *et al.* (Chizhov et al. 2018) proposed a biophysical

516 model (Epileptor-2) of ictal activities based on the Epileptor (Jirsa et al. 2014), using different

517 differential equations. In high potassium conditions, Epileptor-2 produces bursts of bursts,

518 described as ictal-like discharges. However, the most common form of seizure belongs to the

519 saddle-node/homoclinic form, which starts with low voltage fast activity, and ends with bursts

520 slowing down in a logarithmic fashion. The latter was reproduced in the present model,

521 including the period during which neurons stop firing (depolarization block) after seizure onset.

522 Another difference lies in K^+ dynamics. In Epileptor-2, neuronal firing ends when extracellular

523 K^+ returns to baseline level (see Fig 10. in (Chizhov et al. 2018)), whereas in the present model,

524 there is a delay, as consistently found experimentally, as a result of glial cell action. This

525 phenomenon in our model can be visualized by observing the evolution of $[K]_o$ in Fig. 4.

526 Although the Epileptor-2 is not an "intrinsic" Slow/Fast dynamical system, indeed, this model

527 does not describe an independent node as it takes in account the external influence from

528 synaptic inputs from neuronal population. In our model, the observed dynamics, is only due to

529 internal interactions between three compartments.

530   In conclusion, we developed a biophysical model of a single neuron that, despite its

531 simplicity, is able to generate, in a unified framework, many patterns of neuronal network

532 activity found in experimental recording as well as in generic mathematical models. We show

533 that transition from physiological to paroxysmal activity can be obtained by variation of model

534 parameters relating to ion homeostasis while excitability parameters remained constant. Thus,

535 we proposed a simple biophysical model comparable to generic models (El Houssaini et al.

24

536   2015; Jirsa et al. 2014; Saggio et al. 2017), offering the possibility of a biological interpretation

537   of observed dynamics. Neuronal networks increase in complexity from flies to humans, but the

538   basic properties of neurons are roughly conserved. The present study shows that acting on an

539   external variable allows single neurons to go through various patterns of activities, which are

540   also found at the network level in the form of seizures, sustained ictal activity and

541   depolarization block (Cunliffe et al. 2015; Jirsa et al. 2014). We propose that they constitute

542   one of the most primitive forms of activities, appearing as soon as neurons are present.

543

Materials and Methods

545   In this project we aim to build a minimal biophysical model that describes different

546   electrophysiological states of a single neuron, the model is schematized in Fig.1. The model

547   describes three compartments: the intracellular space (ICS), the extracellular (ECS) space and

548   the external bath (EB). Parameters chosen correspond to values observed in whole cell

549   recording. The ion exchange between the ICS and the ECS is carried out by the current flowing

550   through the sodium, potassium, and chloride voltage-gated channels (eq.(5),(6) and (7)), and

551   by the sodium-potassium pump generated current (eq.(8)). Parameters values for these

552   currents have identified in (Hamada et al. 2003; Hille 2001; Läuger 1991) and the membrane

553   capacitance in (Golowasch et al. 2009). Passive diffusion of potassium exists (eq.(4)), between

554   EB and ECS. The EB is mimicking the K+ buffering of vasculature/astrocytes. In ICS and ECS

555   actualization of potassium and sodium concentrations are done (eq.(14)-(20)). The γ

556   parameter has the same unit as the inverse of the Faraday constant, and it is a scaling

557   parameter that permit to include all the mechanisms not detailed in this model which affect the

558   concentration variations (such as co-transporter, exchangers). The values of all the

559   parameters used are given in table 1 and physiological reference and initial values are given

560   in table 2 and table 3.

561

562   **Table 1. Parameters values**

Parameters	Symbol	Value
Membrane capacitance	C_m	1 nF
Gating time constant	τ_n	0.25 ms
Chloride conductance	g_{Cl}	7.5 nS
Maximal potassium conductance	g_K	22 nS
Maximal sodium conductance	g_{Na}	40 nS
Potassium leak conductance	$g_{K,l}$	0.12 nS
Sodium leak conductance	$g_{Na,l}$	0.02 nS
Intracellular volume	ω_i	2160 μm^3
Extracellular volume	ω_o	720 μm^3
Intra/extra cellular volume ratio	$\beta=\omega_i/\omega_o$	3
Conversion factor	γ	0.04 mmole/C.μm^3
Diffusion time constant	ε	0.001 ms^{-1}
Maximal Na/K pump current	ρ	250 pA

571

572   **Table 2. Physiological reference values**

	Ion	Concentration
External bath	$[K]_{bath}$	[2-30] mM
Extracellular	$[K]_{0,o}$	4.8 mM
	$[Na]_{0,o}$	138 mM
	$[Cl]_{0,o}$	112 mM
Intracellular	$[K]_{0,i}$	140 mM
	$[Na]_{0,i}$	16 mM
	$[Cl]_{0,i}$	5 mM

573

574

575   **Table 3. Initial values**

Variable	Initial value
$[K]_o$	$[K]_{0,o}$
$[Na]_o$	$[Na]_{0,o}$
$[Cl]_o$	$[Cl]_{0,o}$
$[K]_i$	$[K]_{0,i}$
$[Na]_i$	$[Na]_{0,i}$
$[Cl]_i$	$[Cl]_{0,i}$
$\Delta[K]_i$	0
$[Kg]$	0
V	-70 mV
n	$n_\infty(-70)$

26

581

582   The model is a slow-fast dynamical system based on 4 equations. The fast system

583   describes the membrane potential eq.(1) and potassium conductance gating variable eq.(2).

584   The slow system describes intracellular potassium concentration variation eq.(3) and

585   extracellular potassium buffering by external bath eq.(4).

586   (1) $\frac{dV}{dt} = -\frac{1}{C_m}(I_{Cl} + I_{Na} + I_K + I_{pump})$

587   (2) $\frac{dn}{dt} = \frac{n_\infty(V) - n}{\tau_n}$

588   (3) $\frac{d\Delta[K]_i}{dt} = -\frac{\gamma}{\omega_i}(I_K - 2 I_{pump})$

589   (4) $\frac{d[K]_g}{dt} = \varepsilon([K]_{bath} - [K]_o)$

590

591   With currents:

592   (5) $I_{Na} = (g_{Na,l} + g_{Na}m_\infty(V)h(n))(V - 26.64\log(\frac{[Na]_o}{[Na]_i}))$

593   (6) $I_K = (g_{K,l} + g_K n)(V - 26.64\log(\frac{[K]_o}{[K]_i}))$

594   (7) $I_{Cl} = g_{Cl}(V + 26.64\log(\frac{[Cl]_o}{[Cl]_i}))$

595   (8) $I_{pump} = \rho\frac{1}{1+\exp(\frac{1}{2}(21-[Na]_i))}\frac{1}{1+\exp(5.5-[K]_o)}$

596   And conductance variables:

597   (9) $n_\infty(V) = \frac{1}{1+\exp(\frac{1}{18}(-19-V))}$

598   (10) $m_\infty(V) = \frac{1}{1+\exp(\frac{1}{12}(-24-V))}$

599   (11) $h(n) = 1.1 - \frac{1}{1+\exp(-8(n-0.4))}$

27

600   The fast subsystem of the model, (eq. (1)&(2)), is a reduction and simplification of

601   conductance-based models, first describe by Hodgkin–Huxley (HH). From the original

602   publication (Hodgkin, A. L., Huxley 1952) the activation variable of K+ channels is determined

603   by the equation (eq.12):

604   (12) $\frac{dn}{dt} = \alpha_n(1 - n) - \beta_n n$

605   Where β(V) and α(V) are the voltage-dependent rate constants determining the probability of

606   transitions between, respectively, opened and closed state of the ion channel. To simplify the

607   model, we propose to describe the variable n, through the voltage-dependent parameter $n_{inf}(V)$

608   and a constant parameter τ_n. In our model, $n_{inf}(V)$ is the probability to find a channel at open

609   state at a given membrane potential while τ_n is the fixed time constant that described the speed

610   for channels to respond to the change of membrane potential. Based on available data in the

611   literature (Bekkers 2000; Hodgkin, A. L., Huxley 1952), and considering that the mean number

612   of channels opened at a given potential is constant, we could qualitatively estimate this

613   relationship (eq.9). In the HH model, the time constant is dependent on the membrane potential

614   due to the formalism used (eq.12). The HH model has been build thanks to experiments done

615   on the squid giant axon, which present differences from on recording of mammalians neurons.

616   We compare the $n_{inf}(V)$ of our model and $1/\tau(V)$, and $n_{inf}(V)$ of the HH model in Fig. 8(a). The

617   shape has been kept from the HH model but starts to increase for lower values of membrane

618   potential. For the voltage-gated sodium channels, variables for opening, m, and for closing, h,

619   have been described(Hodgkin, A. L., Huxley 1952). With the same logic, we can consider the

620   percentage of all population of channels opened. But because this is a very fast mechanism

621   (Hille 2001), it can be considered as an instantaneous function of V (E. Izhikevich 2007)

622   (eq.10). Krinskii and Kokoz (Krinskii,V.I. , Kokoz 1973) showed that n(t)+h(t) is almost constant,

623   so h can be considered as a function of n. Because of the previous modification, we adapted

624   this fitting to obtain the equation of h(n) (eq.11). Due to these simplifications, the

625   interdependence of gating variables makes the spiking rate dependent on τ, as shown in
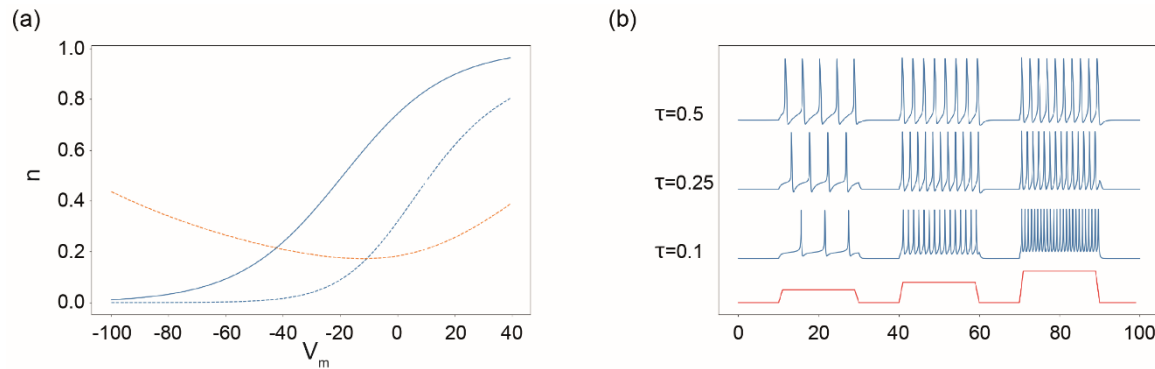
626   Fig.8(b).

28

627

628

629 **Figure 8: modification in gating variables.** (a) n_{inf} of our model in blue, and n_{inf} and $1/\tau$ of the
630 Hodgkin-Huxley model respectively in dash blue and red, function of the membrane potential.
631 (b) Response of the fast subsystem of our model to step current stimulation (red) with three
632 different values of τ (0.1, 0.25, 0.5 ms). The value of τ influence the frequency rate spike for a
633 same injected current.

634

635 To be able to take into account concentration variation limiting the number of equations we

636 applied reductions. Inspired by the work of Hübel (Hübel 2015; Hübel and Dahlem 2014),

637 electroneutrality permits the Eq.(13), and so to the Eq.(14). The ratio $(C_m \gamma)/\omega_i$ is very small

638 ($<10^{-5}$) and so, the right-hand side of Eq.(14) could be considered to be zero. The chloride

639 concentration changes are assumed to be small and regulated by mechanisms which are not

640 described in our model (Doyon et al. 2016). So, in our model, the chloride concentration

641 remains constant.

642 $(13) \dfrac{dV}{dt} = \dfrac{\omega_i}{C_m \gamma} \left(\dfrac{d\Delta[K]_i}{dt} + \dfrac{d\Delta[Na]_i}{dt} + \dfrac{d\Delta[Cl]_i}{dt} \right)$

643 $(14) \Delta[K]_i + \Delta[Na]_i + \Delta[Cl]_i = \dfrac{C_m \gamma}{\omega_i} (V - V_0)$

644

645

646

647

648

29

649   Thanks to these reductions, concentration variations are calculated as follow:

650    $(15) \Delta[Na]_i = -\Delta[K]_i$

651    $(16) \Delta[Na]_o = -\beta \Delta[Na]_i$

652    $(17) \Delta[K]_o = -\beta \Delta[K]_i$

653    $(18) [K]_i = [K]_{0,i} + \Delta[K]_i$

654    $(19) [Na]_i = [Na]_{0,i} + \Delta[Na]_i$

655    $(20) [Na]_o = [Na]_{0,o} + \Delta[Na]_o$

656    $(20) [K]_o = [K]_{0,o} + \Delta[K]_o + [K]_g$

657

658

659   Acknowledgement

667

668

669

References

Barreto, E., & Cressman, J. R. (2011). Ion concentration dynamics as a mechanism for neuronal bursting. *Journal of biological physics*, *37*(3), 361–73. https://doi.org/10.1007/s10867-010-9212-6

Bekkers, J. M. (2000). Distribution and activation of voltage-gated potassium channels in cell-attached and outside-out patches from large layer 5 cortical pyramidal neurons of the rat. *The Journal of physiology*, *525 Pt 3*(Pt 3), 611–20. https://doi.org/10.1111/J.1469-7793.2000.T01-2-00611.X

Bernard, C., Naze, S., Proix, T., & Jirsa, V. K. (2014). Modern concepts of seizure modeling. *International review of neurobiology*, *114*, 121–53. https://doi.org/10.1016/B978-0-12-418693-4.00006-6

Bikson, M., Hahn, P. J., Fox, J. E., & Jefferys, J. G. R. (2003). Depolarization Block of Neurons During Maintenance of Electrographic Seizures. *Journal of Neurophysiology*, *90*(4), 2402–2408. https://doi.org/10.1152/jn.00467.2003

Blenkinsop, A., Valentin, A., Richardson, M. P., & Terry, J. R. (2012). The dynamic evolution of focal-onset epilepsies - combining theoretical and clinical observations. *European Journal of Neuroscience*, *36*(2), 2188–2200. https://doi.org/10.1111/j.1460-9568.2012.08082.x

Bragin, A., Penttonen, M., & Buzsáki, G. (1997). Termination of epileptic afterdischarge in the hippocampus. *The Journal of neuroscience : the official journal of the Society for Neuroscience*, *17*(7), 2567–79. http://www.ncbi.nlm.nih.gov/pubmed/9065516. Accessed 20 January 2019

Chapman, A. G., Westerberg, E., Premachandra, M., & Meldrum, B. S. (1984). Changes in Regional Neurotransmitter Amino Acid Levels in Rat Brain During Seizures Induced by l-Allylglycine, Bicuculline, and Kainic Acid. *Journal of Neurochemistry*, *43*(1), 62–70. https://doi.org/10.1111/j.1471-4159.1984.tb06679.x

Chizhov, A. V., Zefirov, A. V., Amakhin, D. V., Smirnova, E. Y., & Zaitsev, A. V. (2018). Minimal model of interictal and ictal discharges "Epileptor-2." *PLOS Computational Biology*, *14*(5), e1006186. https://doi.org/10.1371/journal.pcbi.1006186

Coulter, D. A., & Steinhäuser, C. (2015). Role of astrocytes in epilepsy. *Cold Spring Harbor perspectives in medicine*, *5*(3), a022434. https://doi.org/10.1101/cshperspect.a022434

Cressman, J. R., Ullah, G., Ziburkus, J., Schiff, S. J., & Barreto, E. (2009). The influence of sodium and potassium dynamics on excitability, seizures, and the stability of persistent states: I. Single neuron dynamics. *Journal of Computational Neuroscience*, *26*(2), 159–170. https://doi.org/10.1007/s10827-008-0132-4

Cunliffe, V. T., Baines, R. A., Giachello, C. N. G., Lin, W. H., Morgan, A., Reuber, M., et al. (2015). Epilepsy research methods update: Understanding the causes of epileptic seizures and identifying new treatments using non-mammalian model organisms. *Seizure*. W.B. Saunders Ltd. https://doi.org/10.1016/j.seizure.2014.09.018

de Almeida, A.-C. G., Rodrigues, A. M., Scorza, F. A., Cavalheiro, E. A., Teixeira, H. Z., Duarte, M. A., et al. (2008). Mechanistic hypotheses for nonsynaptic epileptiform activity induction and its transition from the interictal to ictal state-Computational simulation. *Epilepsia*, *49*(11), 1908–1924. https://doi.org/10.1111/j.1528-1167.2008.01686.x

de Curtis, M., Uva, L., Gnatkovsky, V., & Librizzi, L. (2018). Potassium dynamics and seizures: Why is potassium ictogenic? *Epilepsy Research*, *143*, 50–59.

713   https://doi.org/10.1016/j.eplepsyres.2018.04.005

714   Doyon, N., Vinay, L., Prescott, S. A., & De Koninck, Y. (2016). Chloride Regulation: A Dynamic
715   Equilibrium Crucial for Synaptic Inhibition. *Neuron*, *89*(6), 1157–1172.
716   https://doi.org/10.1016/j.neuron.2016.02.030

717   Dubyak, G. R. (2004). Ion homeostasis, channels, and transporters: an update on cellular
718   mechanisms. *Advances in Physiology Education*, *28*(4), 143–154.
719   https://doi.org/10.1152/advan.00046.2004

720   Durand, D. M., Park, E.-H., & Jensen, A. L. (2010). Potassium diffusive coupling in neural networks.
721   *Philosophical transactions of the Royal Society of London. Series B, Biological sciences*,
722   *365*(1551), 2347–62. https://doi.org/10.1098/rstb.2010.0050

723   During, M. J., & Spencer, D. D. (1993). Extracellular hippocampal glutamate and spontaneous seizure
724   in the conscious human brain. *The Lancet*, *341*(8861), 1607–1610.
725   https://doi.org/10.1016/0140-6736(93)90754-5

726   El Houssaini, K., Ivanov, A. I., Bernard, C., & Jirsa, V. K. (2015). Seizures, refractory status epilepticus,
727   and depolarization block as endogenous brain activities. *Physical Review E*, *91*(1), 010701.
728   https://doi.org/10.1103/PhysRevE.91.010701

729   Fisher, R. S., Pedley, T. A., Moody, W. J., & Prince, D. A. (1976). The role of extracellular potassium in
730   hippocampal epilepsy. *Archives of neurology*, *33*(2), 76–83.
731   http://www.ncbi.nlm.nih.gov/pubmed/1252153. Accessed 12 January 2019

732   Florence, G., Dahlem, M. A., Almeida, A.-C. G., Bassani, J. W. M., & Kurths, J. (2009). The role of
733   extracellular potassium dynamics in the different stages of ictal bursting and spreading
734   depression: A computational study. *Journal of Theoretical Biology*, *258*(2), 219–228.
735   https://doi.org/10.1016/j.jtbi.2009.01.032

736   Fröhlich, F., Bazhenov, M., Iragui-Madoz, V., & Sejnowski, T. J. (2008). Potassium dynamics in the
737   epileptic cortex: new insights on an old topic. *The Neuroscientist : a review journal bringing
738   neurobiology, neurology and psychiatry*, *14*(5), 422–33.
739   https://doi.org/10.1177/1073858408317955

740   Gloveli, T., Albrecht, D., & Heinemann, U. (1995). Properties of low Mg2+ induced epileptiform
741   activity in rat hippocampal and entorhinal cortex slices during adolescence. *Brain research.
742   Developmental brain research*, *87*(2), 145–52. http://www.ncbi.nlm.nih.gov/pubmed/7586496.
743   Accessed 19 January 2019

744   Golowasch, J., Thomas, G., Taylor, A. L., Patel, A., Pineda, A., Khalil, C., & Nadim, F. (2009). Membrane
745   capacitance measurements revisited: Dependence of capacitance value on measurement
746   method in nonisopotential neurons. *Journal of Neurophysiology*, *102*(4), 2161–2175.
747   https://doi.org/10.1152/jn.00160.2009

748   Haglund, M. M., & Schwartzkroin, P. A. (1990). Role of Na-K pump potassium regulation and IPSPs in
749   seizures and spreading depression in immature rabbit hippocampal slices. *Journal of
750   neurophysiology*, *63*(2), 225–39. https://doi.org/10.1152/jn.1990.63.2.225

751   Hamada, K., Matsuura, H., Sanada, M., Toyoda, F., Omatsu-Kanbe, M., Kashiwagi, A., & Yasuda, H.
752   (2003). Properties of the Na +/K + pump current in small neurons from adult rat dorsal root
753   ganglia. *British Journal of Pharmacology*, *138*(8), 1517–1527.
754   https://doi.org/10.1038/sj.bjp.0705170

755   Heinemann, U., Konnerth, A., Pumain, R., & Wadman, W. J. (1986). Extracellular calcium and
756   potassium concentration changes in chronic epileptic brain tissue. *Advances in neurology*, *44*,

757   641–61. http://www.ncbi.nlm.nih.gov/pubmed/3518350. Accessed 23 January 2019

758   Hille, B. (2001). *Ion channels of excitable membranes*. Sinauer.
759   https://global.oup.com/ushe/product/ion-channels-of-excitable-membranes-
760   9780878933211?cc=us&lang=en&#. Accessed 13 January 2019

761   Hodgkin, A. L., Huxley, F. (1952). A quantitative description of membrane current and its application
762   to conduction and excitation in nerve. *J Physiol*, *117*(4), 500–544.

763   Holt, A. B., & Netoff, T. I. (2013). Computational modeling of epilepsy for an experimental
764   neurologist. *Experimental neurology*, *244*, 75–86.
765   https://doi.org/10.1016/j.expneurol.2012.05.003

766   Houssaini, K. El, Bernard, C., & Jirsa, V. K. (2020). The epileptor model: A systematic mathematical
767   analysis linked to the dynamics of seizures, refractory status epilepticus, and depolarization
768   block. *eNeuro*, *7*(2). https://doi.org/10.1523/ENEURO.0485-18.2019

769   Hubbard, J. A., & Binder, D. K. (n.d.). *Astrocytes and epilepsy*.

770   Hübel, N. (2015). *Local dynamics of ion based neuron models for cortical spreading depression, stroke*
771   *and seizures*. Technische Universität Berlin, Fakultät II - Mathematik und Naturwissenschaften.

772   Hübel, N., & Dahlem, M. A. (2014). Dynamics from Seconds to Hours in Hodgkin-Huxley Model with
773   Time-Dependent Ion Concentrations and Buffer Reservoirs. *PLoS Computational Biology*, *10*(12),
774   e1003941. https://doi.org/10.1371/journal.pcbi.1003941

775   Izhikevich, E. (2007). Dynamical Systems In Neuroscience : The Geometry of Excitability and Bursting.
776   *MIT Press*.

777   Izhikevich, E. M. (2000). *NEURAL EXCITABILITY, SPIKING AND BURSTING*. *Tutorials and Reviews*
778   *International Journal of Bifurcation and Chaos* (Vol. 10). http://math.la.asu.edu/. Accessed 13
779   January 2019

780   Jefferys, J. G., & Haas, H. L. (1982). Synchronized bursting of CA1 hippocampal pyramidal cells in the
781   absence of synaptic transmission. *Nature*, *300*(5891), 448–50.
782   http://www.ncbi.nlm.nih.gov/pubmed/6292731. Accessed 13 January 2019

783   Jirsa, Stacey, Quilichini, P. P., Ivanov, A. I., & Bernard, C. (2014). On the nature of seizure dynamics.
784   *Brain : a journal of neurology*, *137*(Pt 8), 2210–30. https://doi.org/10.1093/brain/awu133

785   Jirsa, V.K., Proix, T., Perdikis, D., Woodman, M. M., Wang, H., Gonzalez-Martinez, J., et al. (2017). The
786   Virtual Epileptic Patient: Individualized whole-brain models of epilepsy spread. *NeuroImage*,
787   *145*, 377–388. https://doi.org/10.1016/J.NEUROIMAGE.2016.04.049

788   Jirsa, Viktor K., & Stefanescu, R. A. (2011). Neural Population Modes Capture Biologically Realistic
789   Large Scale Network Dynamics. *Bulletin of Mathematical Biology*, *73*(2), 325–343.
790   https://doi.org/10.1007/s11538-010-9573-9

791   Kager, H., Wadman, W. J., & Somjen, G. G. (2000). Simulated Seizures and Spreading Depression in a
792   Neuron Model Incorporating Interstitial Space and Ion Concentrations. *Journal of*
793   *Neurophysiology*, *84*(1), 495–512. https://doi.org/10.1152/jn.2000.84.1.495

794   Kandel, Eric R., Schwartz James H., Jessell Thomas M., al. (n.d.). *Principles of neural science*.

795   Katayama, Y., Becker, D. P., Tamura, T., & Hovda, D. A. (1990). Massive increases in extracellular
796   potassium and the indiscriminate release of glutamate following concussive brain injury. *Journal*
797   *of Neurosurgery*, *73*(6), 889–900. https://doi.org/10.3171/jns.1990.73.6.0889

798   Kim, C. M., & Nykamp, D. Q. (2017). The influence of depolarization block on seizure-like activity in

33

799   networks of excitatory and inhibitory neurons. *Journal of Computational Neuroscience*, *43*(1),
800   65–79. https://doi.org/10.1007/s10827-017-0647-7

801 Kofuji, P., & Newman, E. A. (2004). Potassium buffering in the central nervous system. *Neuroscience*,
802   *129*(4), 1045–56. https://doi.org/10.1016/j.neuroscience.2004.06.008

803 Krinskii,V.I. , Kokoz, Y. M. (1973). Analysis of equations of excitable membranes-I. Reduction of the
804   Hodgkin-Huxley equations to a second order system. *Biophysica*, *18*, 533–539.
805   https://www.researchgate.net/publication/279566216_Analysis_of_equations_of_excitable_m
806   embranes-I_Reduction_of_the_Hodgkin-Huxley_equations_to_a_second_order_system.
807   Accessed 13 January 2019

808 Krishnan, G. P., Filatov, G., Shilnikov, A., & Bazhenov, M. (2015). Electrogenic properties of the Na^+/K^+
809   ATPase control transitions between normal and pathological brain states. *Journal of*
810   *neurophysiology*, *113*(9), 3356–74. https://doi.org/10.1152/jn.00460.2014

811 Läuger, P. (Peter). (1991). *Electrogenic ion pumps*. Sinauer Associates.

812 Lietsche, J., Imran, I., & Klein, J. (2016). Extracellular levels of ATP and acetylcholine during lithium-
813   pilocarpine induced status epilepticus in rats. *Neuroscience Letters*, *611*, 69–73.
814   https://doi.org/10.1016/j.neulet.2015.11.028

815 Lowenstein, D. H. (2009). Epilepsy after head injury: An overview. *Epilepsia*, *50*, 4–9.
816   https://doi.org/10.1111/j.1528-1167.2008.02004.x

817 Lux, H. D., Heinemann, U., & Dietzel, I. (1986). Ionic changes and alterations in the size of the
818   extracellular space during epileptic activity. *Advances in neurology*, *44*, 619–39.
819   http://www.ncbi.nlm.nih.gov/pubmed/3518349. Accessed 14 January 2019

820 Lytton, W. W. (2008). Computer modelling of epilepsy. *Nature reviews. Neuroscience*, *9*(8), 626–37.
821   https://doi.org/10.1038/nrn2416

822 McCormick, D. A., & Contreras, D. (2001). On The Cellular and Network Bases of Epileptic Seizures.
823   *Annual Review of Physiology*, *63*(1), 815–846. https://doi.org/10.1146/annurev.physiol.63.1.815

824 Merricks, E. M., Smith, E. H., McKhann, G. M., Goodman, R. R., Bateman, L. M., Emerson, R. G., et al.
825   (2015). Single unit action potentials in humans and the effect of seizure activity. *Brain : a*
826   *journal of neurology*, *138*(Pt 10), 2891–906. https://doi.org/10.1093/brain/awv208

827 Meurer, A., Smith, C. P., Paprocki, M., Čertík, O., Kirpichev, S. B., Rocklin, M., et al. (2017). SymPy:
828   symbolic computing in Python. *PeerJ Computer Science*, *3*, e103. https://doi.org/10.7717/peerj-
829   cs.103

830 Miles, R., Blaesse, P., Huberfeld, G., Wittner, L., & Kaila, K. (2012). *Chloride homeostasis and GABA*
831   *signaling in temporal lobe epilepsy*. *Jasper's Basic Mechanisms of the Epilepsies*. National Center
832   for Biotechnology Information (US). http://www.ncbi.nlm.nih.gov/pubmed/22787654. Accessed
833   23 January 2019

834 Millman, K. J., & Aivazis, M. (2011). Python for Scientists and Engineers. *Computing in Science &*
835   *Engineering*, *13*(2), 9–12. https://doi.org/10.1109/MCSE.2011.36

836 Montbrió, E., Pazó, D., & Roxin, A. (2015). Macroscopic Description for Networks of Spiking Neurons.
837   *Physical Review X*, *5*(2), 021028. https://doi.org/10.1103/PhysRevX.5.021028

838 Naze, S. (2015). Multiscale Computational Modeling of Epileptic Seizures : from macro to microscopic
839   dynamics. *Http://Www.Theses.Fr*. https://www.theses.fr/2015AIXM4023

840 Naze, S., Bernard, C., & Jirsa, V. (2015). Computational Modeling of Seizure Dynamics Using Coupled

Neuronal Networks: Factors Shaping Epileptiform Activity. *PLOS Computational Biology*, *11*(5), e1004209. https://doi.org/10.1371/journal.pcbi.1004209

Olsen, M. L., Khakh, B. S., Skatchkov, S. N., Zhou, M., Lee, C. J., & Rouach, N. (2015). New Insights on Astrocyte Ion Channels: Critical for Homeostasis and Neuron-Glia Signaling. *The Journal of neuroscience : the official journal of the Society for Neuroscience*, *35*(41), 13827–35. https://doi.org/10.1523/JNEUROSCI.2603-15.2015

Øyehaug, L., Østby, I., Lloyd, C. M., Omholt, S. W., & Einevoll, G. T. (2012). Dependence of spontaneous neuronal firing and depolarisation block on astroglial membrane transport mechanisms. *Journal of Computational Neuroscience*, *32*(1), 147–165. https://doi.org/10.1007/s10827-011-0345-9

Prinz, A. A., Bucher, D., & Marder, E. (2004). Similar network activity from disparate circuit parameters. *Nature Neuroscience*, *7*(12), 1345–1352. https://doi.org/10.1038/nn1352

Proix, T., Bartolomei, F., Chauvel, P., Bernard, C., & Jirsa, V. K. (2014). Permittivity Coupling across Brain Regions Determines Seizure Recruitment in Partial Epilepsy. *Journal of Neuroscience*, *34*(45), 15009–15021. https://doi.org/10.1523/JNEUROSCI.1570-14.2014

Quilichini, P. P., Diabira, D., Chiron, C., Ben-Ari, Y., & Gozlan, H. (2002). Persistent epileptiform activity induced by low Mg2+ in intact immature brain structures. *The European journal of neuroscience*, *16*(5), 850–60. http://www.ncbi.nlm.nih.gov/pubmed/12372021. Accessed 19 January 2019

Raimondo, J. V., Burman, R. J., Katz, A. A., & Akerman, C. J. (2015). Ion dynamics during seizures. *Frontiers in Cellular Neuroscience*, *9*, 419. https://doi.org/10.3389/FNCEL.2015.00419

Rangroo Thrane, V., Thrane, A. S., Wang, F., Cotrina, M. L., Smith, N. A., Chen, M., et al. (2013). Ammonia triggers neuronal disinhibition and seizures by impairing astrocyte potassium buffering. *Nature medicine*, *19*(12), 1643–8. https://doi.org/10.1038/nm.3400

Reinert, M., Khaldi, A., Zauner, A., Doppenberg, E., Choi, S., & Bullock, R. (2000). High extracellular potassium and its correlates after severe head injury: relationship to high intracranial pressure. *Neurosurgical focus*, *8*(1), e10. http://www.ncbi.nlm.nih.gov/pubmed/16924778. Accessed 13 January 2019

Saggio, M. L., Crisp, D., Scott, J. M., Karoly, P., Kuhlmann, L., Nakatani, M., et al. (2020). A taxonomy of seizure dynamotypes. *eLife*, *9*. https://doi.org/10.7554/eLife.55632

Saggio, M. L., Spiegler, A., Bernard, C., & Jirsa, V. K. (2017). Fast-Slow Bursters in the Unfolding of a High Codimension Singularity and the Ultra-slow Transitions of Classes. *Journal of mathematical neuroscience*, *7*(1), 7. https://doi.org/10.1186/s13408-017-0050-8

Scholl, U. I., Choi, M., Liu, T., Ramaekers, V. T., Häusler, M. G., Grimmer, J., et al. (2009). Seizures, sensorineural deafness, ataxia, mental retardation, and electrolyte imbalance (SeSAME syndrome) caused by mutations in KCNJ10. *Proceedings of the National Academy of Sciences of the United States of America*, *106*(14), 5842–7. https://doi.org/10.1073/pnas.0901749106

Soltesz, I., & Staley, K. (2008). *Computational neuroscience in epilepsy*. Academic. http://booksdescr.org/ads.php?md5=4430D0D436850CEFEB6D8A23B267E8BB. Accessed 19 January 2019

Somjen, G G. (2001). Mechanisms of spreading depression and hypoxic spreading depression-like depolarization. *Physiological reviews*, *81*(3), 1065–96. https://doi.org/10.1152/physrev.2001.81.3.1065

884   Somjen, George G. (2001). Mechanisms of Spreading Depression and Hypoxic Spreading Depression-
885   Like Depolarization. *Physiological Reviews*, *81*(3), 1065–1096.
886   https://doi.org/10.1152/physrev.2001.81.3.1065

887   Staley, K. (2015). Molecular mechanisms of epilepsy. *Nature neuroscience*, *18*(3), 367–72.
888   https://doi.org/10.1038/nn.3947

889   Stefanescu, R. A., Shivakeshavan, R. G., & Talathi, S. S. (2012, December 1). Computational models of
890   epilepsy. *Seizure*. W.B. Saunders. https://doi.org/10.1016/j.seizure.2012.08.012

891   Tankus, A. (2016). Exploring human epileptic activity at the single-neuron level. *Epilepsy & Behavior*,
892   *58*, 11–17. https://doi.org/10.1016/j.yebeh.2016.02.014

893   Traub, R. D., & Wong, R. K. (1982). Cellular mechanism of neuronal synchronization in epilepsy.
894   *Science (New York, N.Y.)*, *216*(4547), 745–7. http://www.ncbi.nlm.nih.gov/pubmed/7079735.
895   Accessed 23 January 2019

896   Traynelis, S. F., & Dingledine, R. (1988). Potassium-induced spontaneous electrographic seizures in
897   the rat hippocampal slice. *Journal of Neurophysiology*, *59*(1), 259–276.
898   https://doi.org/10.1152/jn.1988.59.1.259

899   Traynelis, Stephen F., & Dingledine, R. (1989). Modification of potassium-induced interictal bursts
900   and electrographic seizures by divalent cations. *Neuroscience Letters*, *98*(2), 194–199.
901   https://doi.org/10.1016/0304-3940(89)90509-0

902   Truccolo, W., Donoghue, J. A., Hochberg, L. R., Eskandar, E. N., Madsen, J. R., Anderson, W. S., et al.
903   (2011). Single-neuron dynamics in human focal epilepsy. *Nature neuroscience*, *14*(5), 635–41.
904   https://doi.org/10.1038/nn.2782

905   Ullah, G., & Schiff, S. J. (2010). Assimilating seizure dynamics. *PLoS computational biology*, *6*(5),
906   e1000776. https://doi.org/10.1371/journal.pcbi.1000776

907   Uva, L., Trombin, F., Carriero, G., Avoli, M., & de Curtis, M. (2013). Seizure-like discharges induced by
908   4-aminopyridine in the olfactory system of the in vitro isolated guinea pig brain. *Epilepsia*,
909   *54*(4), 605–15. https://doi.org/10.1111/epi.12133

910   Walz, W. (2000). Role of astrocytes in the clearance of excess extracellular potassium.
911   *Neurochemistry international*, *36*(4–5), 291–300.
912   http://www.ncbi.nlm.nih.gov/pubmed/10732996. Accessed 13 January 2019

913   Wang, L., Dufour, S., Valiante, T. A., & Carlen, P. L. (2016). Extracellular Potassium and Seizures:
914   Excitation, Inhibition and the Role of Ih. *International Journal of Neural Systems*, *26*(08),
915   1650044. https://doi.org/10.1142/S0129065716500441

916   Wang, Y., Trevelyan, A. J., Valentin, A., Alarcon, G., Taylor, P. N., & Kaiser, M. (2017). Mechanisms
917   underlying different onset patterns of focal seizures. *PLOS Computational Biology*, *13*(5),
918   e1005475. https://doi.org/10.1371/journal.pcbi.1005475

919   Wei, Y, Ullah, G., & Schiff, S. J. (2014). Unification of neuronal spikes, seizures, and spreading
920   depression. *J. Neurosci.*, *34*(35), 11733–11743.

921   Wei, Yina, Ullah, G., Ingram, J., & Schiff, S. J. (2014). Oxygen and seizure dynamics: II. Computational
922   modeling. *Journal of neurophysiology*, *112*(2), 213–23. https://doi.org/10.1152/jn.00541.2013

923   Wei, Yina, Ullah, G., & Schiff, S. J. (2014). Unification of Neuronal Spikes, Seizures, and Spreading
924   Depression. *Journal of Neuroscience*, *34*(35), 11733–11743.
925   https://doi.org/10.1523/JNEUROSCI.0516-14.2014

926   Wendling, F., Benquet, P., Bartolomei, F., & Jirsa, V. (2016). Computational models of epileptiform
927   activity. *Journal of Neuroscience Methods*, *260*, 233–251.
928   https://doi.org/10.1016/J.JNEUMETH.2015.03.027

929

930

931

932

933

934

935

936

937

938

939

940

941

942

943

944

945

946

947

Supporting information

S1 Animation. Dynamics of the membrane potential during burst. Considering the two slow variables as parameters of the fast subsystem, fixed point has been found: blue: stable node, green: saddle node, cyan: stable focus, magenta: unstable focus, red: unstable node. The system starts at a stable fixed point and is slowly driven to cross a saddle-node and then follow a limit cycle, until it cross again a saddle-node (creating the Homoclinic bifurcation), and go back to a stable fixed point.

S2 Animation. Dynamic during Burst observed in the phase plane. The n nullcline (blue line) and the V nullcline (blue points) solved numerically. The system starts at a stable fixed point and is slowly driven to cross a saddle-node and then follow a limit cycle, until it cross again a saddle-node (creating the Homoclinic bifurcation), and go back to a stable fixed point.

S3 Animation. Dynamics of the membrane potential during SLEs. Considering the two slow variables as parameters of the fast subsystem, fixed point has been found: blue: stable node, green: saddle node, cyan: stable focus, magenta: unstable focus, red: unstable node. The system starts at a stable fixed point and is slowly driven to cross a saddle-node and then follow a limit cycle, it cross successively two Hopf bifurcations to come back to a limit cycle until it cross again a saddle-node (creating the Homoclinic bifurcation), and go back to a stable fixed point.

S4 Animation. Dynamic during SLEs observed in the phase plane. The n nullcline (blue line) and the V nullcline (blue points) solved numerically the system start at a stable fixed point and is slowly driven to cross a saddle-node and then follow a limit cycle, it cross successively two Hopf bifurcations to come back to a limit cycle until it cross again a saddle-node (creating the Homoclinic bifurcation), and go back to a stable fixed point.